Sensitivity to Z-prime and nonstandard neutrino interactions from ultralow threshold neutrino-nucleus coherent scattering

Bhaskar Dutta, Rupak Mahapatra, Louis E. Strigari, and Joel W. Walker

Phys. Rev. D **93**, 013015 — Published 15 January 2016

DOI: 10.1103/PhysRevD.93.013015

Sensitivity to Z-prime and non-standard neutrino interactions from ultra-low threshold neutrino-nucleus coherent scattering

Bhaskar Dutta[1], Rupak Mahapatra[1], Louis E. Strigari[1], and Joel W. Walker[2]
[1] *Mitchell Institute for Fundamental Physics and Astronomy, Department of Physics and Astronomy, Texas A&M University, College Station, TX 77843-4242, USA and*
[2] *Department of Physics, Sam Houston State University, Huntsville, TX 77341, USA*

We discuss prospects for probing Z-prime and non-standard neutrino interactions using neutrino-nucleus coherent scattering with ultra-low energy ($\sim$ 10 eV) threshold Si and Ge detectors. The analysis is performed in the context of a specific and contemporary reactor-based experimental proposal, developed in cooperation with the Nuclear Science Center at Texas A&M University, and referencing available technology based upon economical and scalable detector arrays. For expected exposures, we show that sensitivity to the Z-prime mass is on the order of several TeV, and is complementary to the LHC search with low mass detectors in the near term. This technology is also shown to provide sensitivity to the neutrino magnetic moment, at a level that surpasses terrestrial limits, and is competitive with more stringent astrophysical bounds. We demonstrate the benefits of combining silicon and germanium detectors for distinguishing between classes of models of new physics, and for suppressing correlated systematic uncertainties.

I. INTRODUCTION

Coherent elastic neutrino-nucleus scattering (CEνNS) is a long-standing prediction of the Standard Model [1], and has been proposed as a new channel to probe neutrino physics and astrophysics [2, 3]. More recently, this process has been identified as the ultimate background to future direct dark matter detection experiments due to neutrinos from the Sun, atmosphere, and supernovae [4–6]. Because of this sensitivity to CEνNS from astrophysically-produced neutrinos, future dark matter detectors may provide a means to probe exotic neutrino properties and interactions [7, 8].

In addition to detectors developed for dark matter searches, several other source and detector configurations have been considered to study CEνNS [9–11]. These include neutrinos from nuclear reactors, intense radioactive sources, or from accelerators. However in spite of the large cross section from CEνNS, enhanced approximately by the square of the number of neutrons in the nucleus, and the sustained experimental effort, CEνNS has yet to be detected. This is primarily because detector technology has been unable to provide sufficiently low threshold sensitivity to register deposition of the kinetic energy of the heavy recoiling nucleus.

In this paper, we discuss the prospects for constraining beyond-the-standard-model (BSM) physics with neutrinos produced from nuclear reactors using new ultra-low threshold ($\sim$ 10 eV) detectors. We investigate different Z' models and compare the reach with the LHC. We probe generic neutrino non-standard interaction (NSI) vertices and explore the reach for the magnetic moment of neutrino. We investigate sensitivity both with and without systematic errors. We study the benefit of combining silicon and germanium detectors, which helps to distinguish between models due to the differential coupling to neutrons and protons. This approach also presents substantial benefits for bypassing the systematic error wall.

Our experimental motivation is direct and imminent, referencing in-hand technology based upon economical and modularly scalable germanium and silicon detector arrays, as elaborated in a parallel publication [12]. Experimental programs that have discussed the prospects for detecting CEνNS from nuclear reactors [13] typically reference nuclear recoil thresholds at the keV scale or greater, and detectors placed $\sim$ 30 m from the reactor core. In contrast, the experimental program that provides motivation for this analysis will be characterized by eV scale nuclear recoil thresholds and closer proximity ($\sim$ 1 m) to the reactor core. We show that these characteristics are expected to enable the first detection of CEνNS, and also facilitate probes of BSM physics.

This paper is organized as follows. In Section II, we review properties of the proposed nuclear reactor site and contextualize the experiment in terms of other efforts toward the detection of CEνNS. In Section III, we review the physics of neutrino-nucleus coherent scattering. In Section IV, we discuss sensitivity to Z'-mediated interactions. In Section V, we discuss sensitivity to non-standard neutrino interactions. In Section VI, we explore the benefits of comparing scattering rates from different nuclei to the suppression of systematic errors. In Section VII, we present our conclusions.

II. REACTOR PROPERTIES AND EXPERIMENTAL CONTEXT

The current analysis is performed in the context of a specific and contemporary experimental proposal, developed in cooperation with the Nuclear Science Center at Texas A&M University (TAMU), which administrates a megawatt-class TRIGA-type pool reactor stocked with low-enriched ($\sim 20\%$) ^{235}U. Tight physical proximity of the experimental apparatus to the reactor core can be maintained, and we will reference a baseline separation of 1 m; the installed distance to core is expected to be within the range of 1-3 m. This adjacency geometrically enhances the neutrino flux to a level order-comparable with that typifying experiments at a 30 m baseline from a gigawatt-class power reactor source. Reactor operators are able to provide high-precision measurements of the thermal output power, as well as estimates (based on simulation with the code `MCNP` [14]) of the isotopic fuel composition and fission fractions f_i/F, where f_i is the absolute fission rate of species i and $F \equiv \sum f_i$. Neutrino data will be collected in both on and off reactor modes, and with variations in the position of the (rail-mounted) reactor core, in order to facilitate precise estimates of the background rate. The concurrent observation of residual gamma and neutron events will provide an independent handle for estimating the underlying neutrino flux.

Thermal power is generated in the reactor by fission, via neutron capture, of the nuclei ^{235}U, ^{238}U, ^{239}Pu, and ^{241}Pu. The common isotope ^{238}U (with a half-life comparable to the age of the Earth) is not readily fissile by thermal neutrons, but will split upon fast neutron capture. Capture of thermal neutrons will typically induce breeding to ^{239}U, which proceeds in two steps by β-decay (with a half life of 23 minutes and 2.4 days, respectively) to ^{239}Np and then ^{239}Pu. This breeding process also contributes subdominantly to the reactor thermal power, and appreciably to the anti-neutrino flux. In addition to its own fission process, ^{239}Pu will similarly exhibit breeding, by double neutron capture, to ^{241}Pu. The α-decay of ^{239}Pu back to ^{235}U is comparatively slow, with a half life around 24,000 years.

The TAMU reactor thermal power $W_{\rm Th} = 1.00 \pm 0.02$ MW (established by thermodynamic balance) may be combined with the relevant fission fractions in order to establish the intrinsic anti-neutrino flux. The thermal energy $E_{\rm Th}$ (not counting escaping neutrinos, but incorporating recapture of neutrons not active in down-stream fission events) released per fission (on the order of 200 MeV) for the primary reactor constituents [15] are presented in Table I. Since the thermal output is integrated over the cascaded decay of all sequential daughter products, some of which are relatively long-lived, these rates are likewise mildly dependent upon the reactor fuel evolution, and typical mid-cycle values are tabulated. Also included in Table I are the mean cumulative energy $\langle E_\nu \rangle$ per fission delivered to neutrinos [15], the mean number $\langle N_\nu \rangle$ of neutrinos sharing that energy budget in the decay cascade [16], and typical fission fractions f_i/F of the TAMU research reactor (cf. Ref. [17] for the rates $0.56 : 0.07 : 0.31 : 0.06$ in a representative power reactor, where the concentration and fission of ^{239}Pu is much more substantial). The average neutrino fission product is boosted to about 1.5 MeV, although energies of 10 MeV and beyond are possible. An effective fission fraction of about 0.16 (in comparison to about 0.6 in a typical power reactor context [17]) may be attributed to the non-fission $^{238}\text{U} \to {}^{239}\text{Pu}$ breeding process; this term is not included in the normalization F.

TABLE I: Thermal energy released per fission, average cumulative neutrino energy per fission, average count of cascaded neutrino emissions per fission, and typical fission fraction in the TAMU research reactor are provided for the primary fissile fuel components (along with effective values for the non-fission uranium to plutonium breeding process). Dimensionful quantities are reported in MeV.

Nucleus	$E_{\rm Th}$	$\langle E_\nu \rangle$	$\langle N_\nu \rangle$	f_i/F
^{235}U	201.92 ± 0.46	9.07 ± 0.32	6.14	0.967
^{238}U	205.52 ± 0.96	11.00 ± 0.80	7.08	0.013
^{239}Pu	209.99 ± 0.60	7.22 ± 0.27	5.58	0.020
^{241}Pu	213.60 ± 0.65	8.71 ± 0.30	6.42	< 0.001
$^{238}\text{U} \to {}^{239}\text{Pu}$	1.95	1.2	2.0	0.16

Averaging over fission fractions (which are presently dominated by ^{235}U), and momentarily neglecting the breeding of ^{238}U, a thermal energy per fission of about 202 MeV is expected, with 6.1 anti-neutrinos carrying a net invisible energy of 9.1 MeV. At a reactor power of 1.0 MW, the extrapolated fission rate is 3.1×10^{16} s^{-1} with an intrinsic anti-neutrino production rate of 1.9×10^{17} s^{-1}, and a fission anti-neutrino flux of $\Phi_\nu^{\rm f} = 1.5 \times 10^{12}$ cm^{-2}s^{-1} at a mean distance from core of 1 m. If ^{238}U breeding carries an effective fission fraction of 0.16, with 2 anti-neutrino emissions per neutron capture, then there is a second contribution to the flux of $\Phi_\nu^{\rm b} = 7.9 \times 10^{10}$ cm^{-2}s^{-1} with a relative strength of about 5%, but with a much more focused presentation in the low-energy regime. These fluxes are reduced by a factor of 4 with the $1/r^2$ dilution at a distance from core of 2 m, or a factor of 9 at 3 m. There is additionally a subdominant solar neutrino component.

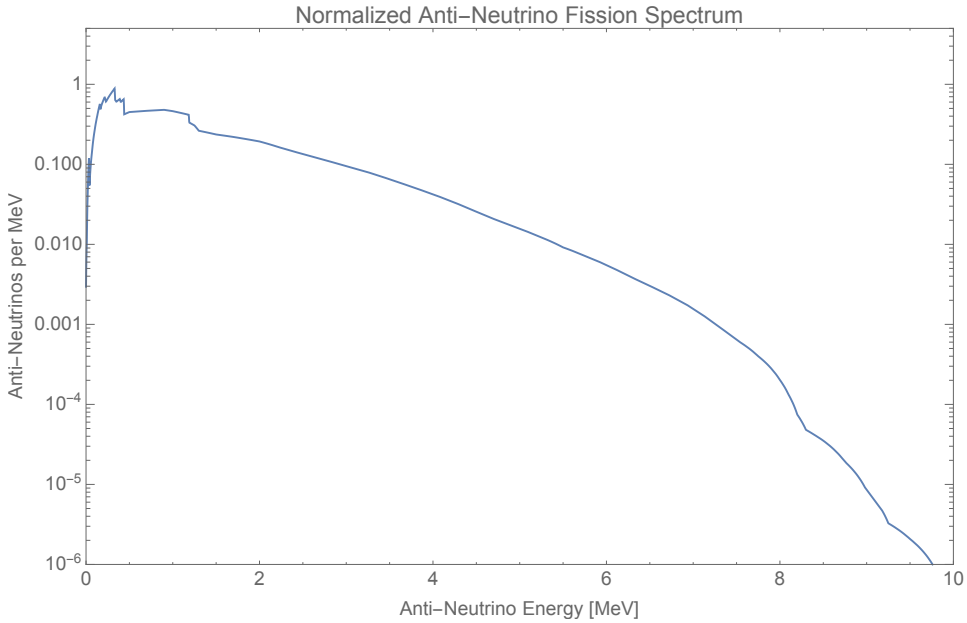

FIG. 1: Normalized anti-neutrino fission spectrum [17, 18] employed in the present study.

In the uranium to plutonium breeding reaction, an energy of about 2 MeV is released (about one percent of that from a typical fission), with just under two-thirds associated with the first (uranium to neptunium) β-transition. The shape of the anti-neutrino energy spectrum is modeled by the Fermi theory (cf. Ref. [19] and references therein), with a functional form $E_\nu^2(Q-T_e)^2$ (where Q is the energy yield, T_e the electron kinetic energy, and E_ν the neutrino energy) modified by a term representing the Coulomb drag of the nucleus potential. The average anti-neutrino energy budget for the two decays (as a sum) is about 1.2 MeV, which gives each of the two decays less than half the energy typical of a fission process. Additionally, the normalized energy spectrum declines precipitously above about 1.5 MeV, lacking the long tail feature exhibited by the fission products. This imparts a distinct low-energy edge characteristic to the unified anti-neutrino spectrum, which may be probed by an appropriately low-threshold detector. In general, the absence of experimental data below $E_\nu = 2$ MeV is, in itself, a motivation for direct measurements of the neutrino nuclear recoil at extraordinarily low activation thresholds.

A classic series of reactor experiments and analyses [16, 18, 20, 21] performed during the 1980's are the standing primary references for numbers on the normalization and detailed spectral distribution of neutrino daughter products; a more recent reinterpretation of the historical data was presented in Ref. [22]. To be concrete, all modeling in the present study will adopt standardized tabulated spectra. Below 2 MeV (the inverse β-decay $\overline{\nu}_e + p \to e^+ + n$ threshold is $E_\nu > 1.8$ MeV) there is no experimental data, and we will employ the theoretically established curve of Ref. [17], which assumes typical power reactor distributions for each of the Table I processes. Above 2 MeV, we will employ the spectrum of Ref. [18], which is extrapolated from direct observation of positron emission in ^{235}U. Experiment and theory agree on the integrated flux at better than 2% above the inverse β-decay threshold [17, 23]. The resulting unified spectrum is presented graphically as Fig. (1).

There are several other existing experimental proposals (cf. Ref [24]) for measurement of the CEνNS process, which employ various modes of neutrino production. We summarize here a few relevant examples, emphasizing similarities and differences as well as advantages and disadvantages of the various approaches. The COHERENT [25] project is designed around the use of a stopped-pion neutrinos derived from the Spallation Neutron Source at Oak Ridge National Laboratory. This production mode generates prompt muon neutrinos, as well as delayed electron neutrinos and muon anti-neutrinos, in contrast to the pure electron anti-neutrino content expected at a reactor source. This fact implies that distinct interaction vertices may be probed in a complementary manner. Also, the pulsed timing of the beam yields substantial advantages for the reduction of asynchronous backgrounds. Moreover, the typical neutrino energy is above 30 MeV, which is a factor of twenty or more larger than the mean energy at a reactor. Since the integrated cross section scales as E_ν^2 both the event rate at fixed flux and the minimal recoil threshold are simultaneously elevated by a factor in the neighborhood of 500. In particular, this means that less exotic detectors, including non cryogenic scintillators, may be considered. However, the expected neutrino flux is substantially lower than at a reactor, on the order of a few times $10^7/\mathrm{cm}^2/\mathrm{s}$ at a range of 20 [m] from the target. In particular, this is down by about five orders of magnitude from the expected output of the TAMU reactor at one meter. The advent of

suitably low-threshold detectors thereby tilts the advantage in expected CEνNS event rate per kilogram back toward reactor-based sources by as much as a few hundred-fold. There are also proposals for accelerator-based stopped pion sources, such as the DAEδALUS [26] experiment, which have essential similar characteristics. The proposed liquid argon detector in that experiment is projected to register approximately 10 CEνNS events per kilogram per year, a figure that is suppressed by up to three magnitude orders relative to the projections in the present work. Candidates for reactor-based CEνNS observation include the TEXONO [27, 28] and CoGeNT at SONGS projects. All such reactor based environments feature an essentially identical electron antineutrino spectrum. Potentially distinguishing features including the reactor power, the distance from core, and the recoil threshold sensitivity. The TEXONO experiment is housed at the Kuo-Sheng power reactor in Taiwan, which operates in the typical few gigawatt power range. At thirty meters from core, it yields a flux that is broadly comparable to (or perhaps larger by a few times than) that available at our referenced megawatt research reactor at one meter from core. The SONGS facility also employs a research reactor, albeit one generating approximately 30 megawatts of power. With the detector placed 20 meters from core, this corresponds to a net reduction of one magnitude order in flux relative to our proposal at one meter from core, or flux parity at three meters from core. Both projects are likewise actively pursuing low noise germanium detection environments capable of reaching recoil thresholds in the one-to-a-few hundreds of eV range [29, 30]. Our referenced ^{72}Ge and ^{28}Si detector technology is capable of substantially broaching the 100 eV threshold, plausibly reaching as low as 10 eV, in the very near term future [12].

III. NEUTRINO-ATOM SCATTERING

The standard model (SM) electroweak Lagrangian exhibits the gauge symmetry $SU(2)_L \times U(1)_Y$, with gauge fields W^i_μ and B_μ, and couplings g and g', respectively. After electroweak symmetry breaking, the residual symmetry is $U(1)_{EM}$, with coupling $e \equiv g \sin\theta_W$, where the Weinberg angle is defined by the relation $\tan\theta_W \equiv g'/g$. The massive neutral current is mediated by the mixed bosonic state Z_μ, with an effective coupling (conventionally defined as) $g/\cos\theta_W$ and an associated charge operator $T_3 - Q_{EM}\sin^2\theta_W$, where T_3 is the diagonal generator of $SU(2)_L$, with eigenvalues $\pm 1/2$ for the upper and lower components of a field doublet, respectively.

For small momentum exchange, the Z_μ propagator will be dominated by its M_Z^2 mass-denominator, generating an effective (mass-suppressed) dimension-six coupling $G_F \equiv \sqrt{2}g^2/8M_W^2$, where $M_W \equiv M_Z \cos\theta_W$. The differential cross-section [31] for SM scattering of a neutrino with energy E_ν from a target particle of mass M and kinetic recoil $T_{\rm R}$ is, in terms of the applicable vector $q_V \equiv q_L + q_R$ and axial $q_A \equiv q_L - q_R$ charges,

$$\frac{d\sigma}{dT_{\rm R}} = \frac{G_F^2 M}{2\pi}\left[(q_V+q_A)^2 + (q_V-q_A)^2\left(1-\frac{T_{\rm R}}{E_\nu}\right)^2 - (q_V^2-q_A^2)\frac{MT_{\rm R}}{E_\nu^2}\right]. \quad (1)$$

Eq. (1) is applicable both to scattering from electrons and to scattering from nuclei. The SM neutrino is purely left-handed, but couples via the Z-boson neutral current (with distinct strengths) to both left- and right-handed fermionic currents. By convention, the global contribution (a factor of 1/2) to the neutral-current vector and axial charges from the pure-left neutrino has been factored out, such that the referenced charges (and L/R chirality designations) refer only to the scattering host.

For (e, ν_e) scattering, the flavor-diagonal t-channel exchange of a W-boson interferes with the neutral current term, effectively boosting (q_V, q_A) by a unit value [31]. This diagram is not applicable, though, to the scenario of a reactor anti-neutrino source. However, there is a second subtlety that is relevant in this case, namely the emergence of a relative negative phase between (q_V, q_A) associated with the parity-flip. Absorbing this sign into the axial coupling, the SM expressions for anti-neutrino scattering from a generic fundamental particle target become $(q_V, q_A) \equiv (T_3 - 2Q\sin^2\theta_W, -T_3)$. For coherent nuclear scattering, these terms should be summed over the quark content of protons and neutrons, and either multiplied by the respective counts (Z, N) of each (in the vector case) or multiplied by the respective differential counts $(Z^+ - Z^-, N^+ - N^-)$ of up and down spins (in the axial case) [32]. The leading event contribution comes from the neutron count N, with $q_V^N = -0.5$ (independent of the Weinberg angle), whereas coupling to the proton $q_V^P \simeq +0.038$ experiences strong interference and is relatively suppressed by more than a magnitude order.

The described sum over nuclear constituents at the coupling level, prior to squaring in the amplitude, is the essence of the nuclear coherency boost. By contrast, electron scattering sums over the atomic number Z incoherently, boosting the cross-section linearly rather than quadratically. We note as a curiosity that further reduction of the neutrino energy (to around the milli-eV scale) induces coherency at the level of electron scattering [33]. Both of the suggested target nuclei, namely ^{72}Ge and ^{28}Si, have a total spin of zero, although the germanium nucleus has a deficit of spin-up protons (and an excess of spin-up neutrons) of two units, which is observed to boost the expected scattering count by about 3.5% relative to the dominant vector mode. There are calculable correction factors that account for

the eV-scale binding energy of scattered electrons, which we neglect in comparison to the MeV-scale energy of the reactor anti-neutrino source. Another subleading effect that that could contribute meaningful systematics on the order of targeted signals of new physics is the excitation of low-lying nuclear states. We generally expect charged current, incoherent, and inelastic scattering cross sections to increase more rapidly with energy than the CEνNS cross section [34], such that these effects are substantially suppressed for reactor-scale neutrino energies in the few MeV range. In keeping, we find the calculable form factors [35] that gauge applicability of the nuclear coherency assumption to be of unit value within a part per few thousand at typical reactor neutrino energies, and consequently further neglect their consideration here. Incidentally, such effects may be more problematic (or one may have greater opportunity to probe structure of the nuclear form factor) with a higher energy neutrino source, e.g. a stopped pion beam. Radiative corrections to the sine-squared Weinberg angle and the neutral current couplings [36] have been included in leading terms.

It is clear that nuclear scattering will generally be dominated by the vector charge, and in the limit of vanishing axial charge the residual functional dependence $1 - MT_{\rm R}/2E_\nu^2$ interpolates between a large cross-section at zero recoil and a vanishing cross-section at cut-off, where energy-momentum conservation stipulates the maximum recoil $T_{\rm R}^{\rm max} = 2E_\nu^2/(M + 2E_\nu)$ achievable in a collision with no glancing component. The large mass-denominator in this term highlights the necessity of ultra-low threshold detectors for observation of the heavily boosted CEνNS feature. We calculate that a detector threshold around 50, 20 eV is required in ^{28}Si, ^{72}Gein order to capture about half of the scattering from fission neutrinos with a mean energy of 1.5 MeV, as demonstrated graphically in Figs. (2). We note additionally that the area under the $1-T_{\rm R}/T_{\rm R}^{\rm max}$ curve is $T_{\rm R}^{\rm max}/2 \simeq E_\nu^2/M$, which yields the previously quoted scaling with regards to the incident neutrino energy, and the associated prospect that higher values of E_ν may partially offset very stringent recoil threshold requirements.

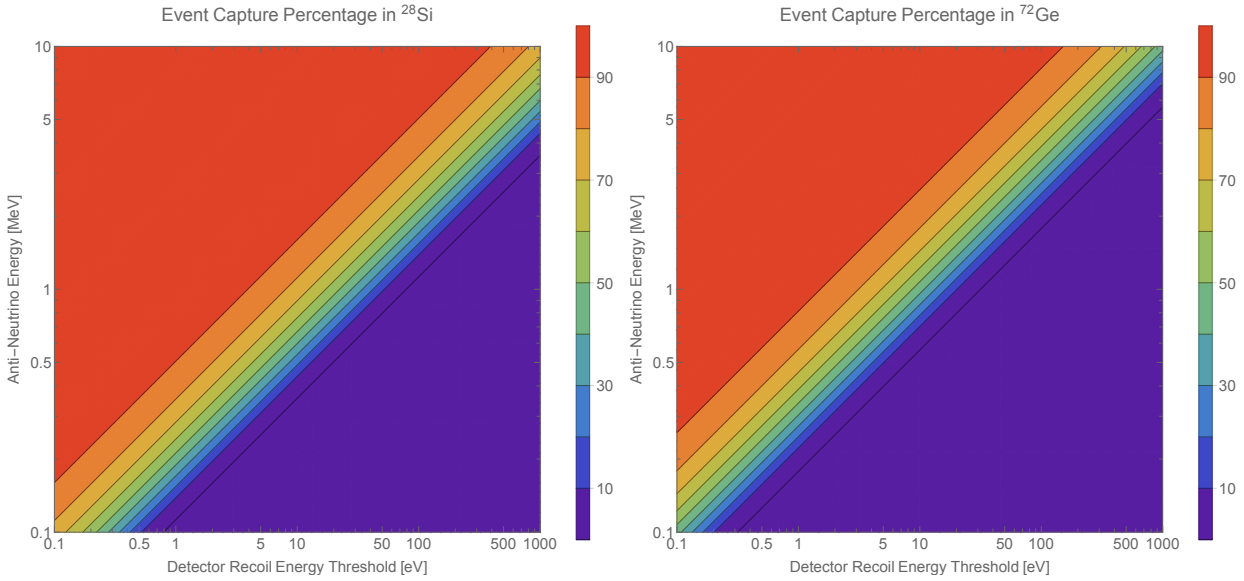

FIG. 2: Percentage of nuclear recoils captured by ^{28}Si and ^{72}Ge detectors as a function of the incident anti-neutrino energy E_ν and the recoil threshold $T_{\rm R}^{\rm th}$.

If the neutrino has a non-vanishing magnetic moment μ_ν (expressed dimensionlessly as a multiple of the Bohr magneton $\mu_{\rm Bohr} \equiv e/2m_e$), then this supplements (as a simple sum) the scattering cross section(s) described in Eq. (1) [31],

$$\left.\frac{d\sigma}{dT_{\rm R}}\right|_{\mu_\nu} = \frac{\pi\alpha^2\mu_\nu^2}{m_e^2}\left[\frac{1 - T_{\rm R}/E_\nu}{T_{\rm R}} + \frac{T_{\rm R}}{4E_\nu^2}\right]. \tag{2}$$

The second term of Eq. (2) applies only to the case of nuclear scattering, while both nuclear and electron scattering reference the first term. For coherent nuclear scattering, the unified contribution will again be multiplied by Z^2, whereas the sum over individual elements of the electron cloud is again linear, providing a factor of just Z. For nuclei with odd atomic number there are additional terms dependent upon the nuclear magnetic moment [31].

In order to compute the cumulative expected Standard Model anti-neutrino capture (cf. Ref [32]), it is necessary to integrate in the region of the E_ν vs. $T_{\rm R}$ plane that is above $E_\nu > E_\nu^{\rm min} = (T_{\rm R} + \sqrt{2MT_{\rm R} + T_{\rm R}^2})/2$, which is the minimal neutrino energy (i.e. the inversion of the expression for $T_{\rm R}^{\rm max}$) required to trigger a given recoil, and

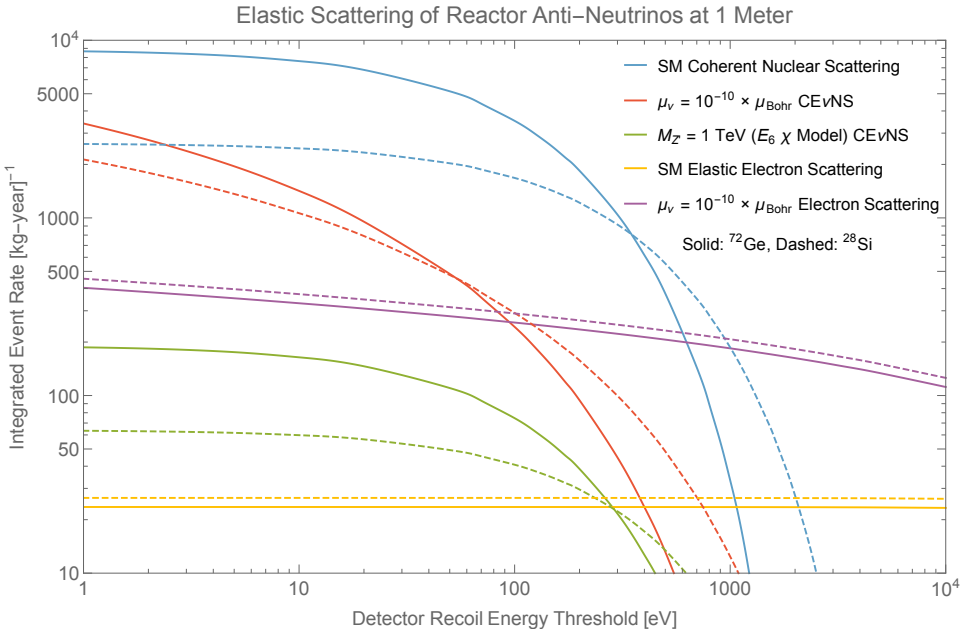

FIG. 3: Integrated yield of nuclear recoil events (per kg per year) captured by ^{72}Ge (solid) and ^{28}Si (dashed) detectors as a function of detector recoil threshold $T_{\rm R}^{\rm th}$. Independent curves are exhibited for the contribution of nuclear and electron cloud recoils, and for benchmark Z' and neutrino magnetic moment μ_ν scattering. This plot cannot be used to compare visibility of magnetic moment and Z' searches, as both use an arbitrarily established benchmark value.

for $T_{\rm R} > T_{\rm R}^{\rm th}$ of the detector recoil threshold. The integrand is a product of the previously described differential cross section and the normalized anti-neutrino energy spectral distribution $dN_\nu/dE_\nu \div N_\nu$, as well as the ambient anti-neutrino flux, the detector mass, and the exposure time.

Fig. (3) exhibits primary results for the expected event capture rate, as a function of the detector recoil threshold $T_{\rm R}^{\rm th}$, for both ^{72}Ge (solid curves) and ^{28}Si (dashed curves), per kilogram, per year. Separate curves are presented for nuclear and electron recoils, for the magnetic moment contribution (at a benchmark value of $\mu = 10^{-10}$), and for the enhancement expected from existence of a Z' gauge boson (using a benchmark E_6 "χ" model with $M_{Z'} = 1$ TeV), the treatment of which are described in detail subsequently. The electron curves all flatten out at much larger thresholds, due to the denominator $M + 2E_\nu$ in the maximum recoil. It is clear that SM elastic scattering from the electron cloud is important at super-keV thresholds, but is completely lost relative to the emergence of the CEνNS at low thresholds. The magnetic moment contribution is larger in terms of absolute numbers for the nucleus, although it is a more relevant fractionally for the electrons. The recoil threshold $T_{\rm R}^{\rm th}$ contributes in the denominator of a logarithm to the integrated event rate for the magnetic moment scattering, which explains the steepness of the observed slope for the red CEνNS curves. There is also a mass denominator inside this logarithm that suppresses the nuclear magnetic moment scattering, but the enhancement for the electrons is regulated by a sum with the neutrino energy, and its effect is limited. It cannot overcome the coherent nucleon-squared enhancement that sits outside the logarithm for the nuclear case. Electron magnetic moment scattering is comparable to nuclear magnetic moment scattering at a threshold around 100 eV, the nuclear term dominates by a factor of about 5 around 10 eV, and a factor of about 10 at 1 eV. The benefit of low thresholds to the observation of magnetic moment interactions is thus very clear, and even more so than for Z' scattering, with event rates rising much faster in this regime than for all other CEνNS processes.

IV. SENSITIVITY TO Z-PRIME INTERACTIONS

In this section, we discuss prospects for constraining Z' interactions [37–40] using ultra-low energy threshold Si and Ge detectors [9]. Heavy analogs of the Z boson are a mainstay of BSM physics, associated with extra local $U(1)$ symmetries that arise naturally in various string theoretic and grand unified theory (GUT) constructions. The presence of a heavy neutral Z' gauge boson would manifest itself as a modification (generally enhancement) in the rate of detected anti-neutrino scattering events. Specifically, the SM vector and axial charges are summed (there can be interference) with contributions to (q_V, q_A) from the new physics, which will necessarily carry the dependence $(M_Z/M_{Z'})^2$, reflecting modification of the propagator to the Fermi coupling. The event rate is proportional to the

charge-squared, and the new physics will manifest primarily via a cross-term with the much larger SM charges, such that the expected signal event rate declines still as just $1/M_{Z'}^2$. Also of potential interest, although beyond the present scope, is the possibility of light Abelian vector bosons with Stueckelberg mass generation [41, 42].

In order to formulate a charge factor for the new physics that sums correctly with the SM terms, several normalization coefficients must be computed. In full, the prescription for a scattering from a target i will be

$$Q_{SM}(i) \;\Rightarrow\; Q_{SM}(i) \,+\, Q_{\rm BSM}(i) \;\times \left\{ Q_{\rm BSM}(\nu)/Q_{\rm SM}(\nu) \times (g' \,\cos\theta_W/g)^2 \;\times (M_Z/M_{Z'})^2 \right\},$$

where previously described global coupling, charge, and mass terms that were explicitly factored out in the SM analysis have been exchanged for the appropriate BSM analogs; g' is the BSM hypercharge, and we assume a decoupling limit where the heavy Z' does not mix in the electroweak symmetry breaking.

In order to broadly assess the sensitivity of a solid state detector to these heavy particles, we consider five benchmark Z' models that are representative of the most common approaches to this idea. Two of the benchmarks will be taken from the symmetry breaking of a typical string-derived scenario featuring the unified E_6 group. In this scenario, two $U(1)$ factors may combine via an unspecified mixing angle β to generate a single TeV-scale gauge field. The most studied mixing angles are $\beta = 0$ (χ model), $\beta = \cos^{-1}\sqrt{3/8}$ (η model), and $\beta = \pi/2$ (ψ model). Silicon and germanium detectors are not sensitive to the ψ model, which features purely axial couplings. Two additional benchmarks are associated with models invoking a baryon minus lepton $B - L$ symmetry [43, 44]. As this is not a unified theory, the coupling strength is arbitrary, and we consider both ($g' = 0.4$) and ($g' = 0.2$) examples, the former being near to the limit allowed by high-energy consistency of the renormalization group. The final model considered is a toy model called the sequential standard model (SSM), whose couplings are identical to those of the Z-boson after electroweak symmetry breaking.

Table II itemizes the quark and lepton neutron current charges in the SM (equivalently SSM), and the various described extensions [40, 43, 45]. In the E_6 models, $(g'/g)^2$ is fixed to be $\frac{5}{3}\tan^2\theta$, where the factor of 5/3 preserves proper GUT charge normalization. In the $B - L$ models, (g'/g) is not constrained, and the coupling g' is generally provided explicitly; the $SU(2)_L$ coupling is given numerically by $g \simeq 0.65$. In the sequential standard model, $(g' \cos\theta_W/g)^2 = 1$. Continuous parameterization of E_6 models is provided by the definition $Q_{E_6} \equiv \cos\beta\, Q_{E_6}^{\chi} + \sin\beta\, Q_{E_6}^{\psi}$. As before, the unified axial charge q_A will inherit a relative sign-flip for the scenario of anti-neutrino scattering, after summation of all relevant contributions.

TABLE II: Quark and lepton neutral current charges in the SM and various extensions.

	Q_{SM}	$\sqrt{40}\,Q_{E_6}^{\chi}$	$\sqrt{24}\,Q_{E_6}^{\psi}$	Q_{B-L}
u_L	$\frac{1}{2} - \frac{2}{3}\sin^2\theta_W$	-1	1	$\frac{1}{3}$
d_L	$-\frac{1}{2} + \frac{1}{3}\sin^2\theta_W$	-1	1	$\frac{1}{3}$
u_R	$-\frac{2}{3}\sin^2\theta_W$	1	-1	$\frac{1}{3}$
d_R	$\frac{1}{3}\sin^2\theta_W$	-3	-1	$\frac{1}{3}$
ν_L	$\frac{1}{2}$	3	1	-1
e_L	$-\frac{1}{2} + \sin^2\theta_W$	3	1	-1
e_R	$\sin^2\theta_W$	1	-1	-1

We note that bounds on the Z' from CEνNS are complementary to those obtained from the LHC, which probes for resonance peaks in the dilepton invariant mass. Whereas a collider is directly sensitive to the Z' mass scale, individual coherent nuclear recoil events cannot tag the mass of the mediating species. Still, the coherency boost at very low recoil thresholds can allow for exquisite statistical sensitivity to the Z' scale. Projected 95% confidence limits on the Z' mass at the $\sqrt{s} = 13/14$ TeV LHC with a few (1-3) hundreds of events per femtobarn of luminosity are in the range of 5 to 6 TeV [44, 45] for the described benchmark scenarios. Limits for the $B - L$ model go as (6,5,4.4) TeV for couplings g' of (0.4,0.2,0.1), respectively. The naive proportional scaling of the mass limit with the g' coupling is not realizable in a collider scenario, where mass suppression of the parton luminosity at high momenta inhibit the reach into heavier models. The solid state detectors do not exhibit this shortcoming, being sensitive to the Z' mass only in the off-shell Fermi-coupling sense, and thus fare proportionally better at large coupling.

In order to concretely assess event detection significance, we select the signal S to background B significance metric $S/\sqrt{B}$. Both S and B scale linearly with luminosity $\mathcal{L}$, and S additionally scales proportionally with $1/M_{Z'}^2$. At fixed significance $S/\sqrt{B}$, the mass reach for nuclear recoil detectors will thus scale like $M_{Z'}^{\rm Lim} \propto \mathcal{L}^{1/4}$ i.e. a fourth-root

of the product of neutrino flux, exposure time, and detector mass. Projected mass exclusions at 95% confidence (statistical only, single-sided) for each benchmark model are provided as a function of the detector recoil threshold $T_{\rm R}^{\rm th}$ in Fig. (4). The benchmark early phase detector is composed of ^{72}Ge and ^{28}Si in roughly a 2:1 mass ratio, with a combined mass of 30 kg, operating for a one-year continuous exposure, at 1 m from core. Bounds are in the range of 1.8 to 2.4 TeV for most models, reaching above 4 TeV for the strongly-coupled $B-L$ model. Expanding upon this example, scaling up to 5 ton-years or 100 ton-years would increase the bounds by factors of almost 4 and 8, respectively. This suggests that a low threshold CEνNS measurement could be competitive with the foreseeable collider reach, and even substantially exceed it, given sufficient scaling of the experiment.

However, a full analysis of the Z' scale bounds from CEνNS will necessarily be dominated by statistical uncertainties. Although detection efficiency above threshold and within the fiducial volume approaches 100%, with controllable backgrounds, and vanishing pile-up (milli-second recovery time), the dominant uncertainty will be propagated from errors in the reactor thermal power, and from the extrapolation of this power into the associated anti-neutrino spectrum. Uncertainty estimates on the order of 2% are typical, although it may be possible to reduce this to around a half of a percent (cf. Ref. [46]).

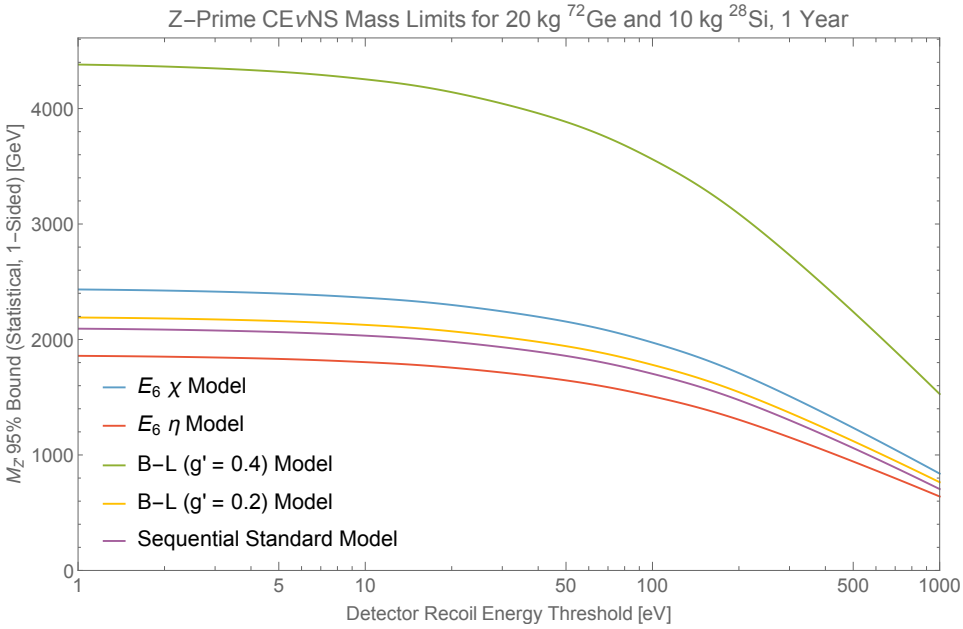

FIG. 4: Sensitivity to Z' in different models.

In Fig. (5), we show the BSM event fraction for various Z' models, as a function of $M_{Z'}$, which should not be less than the order of the anticipated systematic uncertainties. Such fixed percentile errors will do more damage in the large detector mass and high luminosity regimes, where statistical fluctuations are tailing off as a percentage of events. This does not, however, imply that additional statistical resolution is without benefit. Since various Z' models couple distinctly to up and down quarks, differential and rational event counts in detectors with contrasting atomic and mass numbers, such as ^{72}Ge and ^{28}Si, can be very sensitive to deviations from the standard model in a manner that cancels leading systematic uncertainties. This sensitivity to the *existence and mode* of new Z' or μ_ν physics, even more so than the scale, is a key distinguishing benefit nuclear recoil detectors over other approaches [32], as will be further elaborated in the final section.

We close this section by noting that ATLAS [47] has recently reported excesses in searches for massive resonances decaying into a pair of weak gauge bosons, and CMS [48] also has reported a diboson excess. One suitable explanation exists in the context of a leptophobic $SU(2)_L \times SU(2)_R \times U(1)_{B-L}$ model [49]. The prediction arising from this model is a 3-5 TeV Z' that couples to SM leptons as shown in Ref. [49]. This sort of field is potentially well-suited for study via the CEνNS approach, especially with regards to the probing its characteristic mode of coupling to up- and down-quarks. Such complementary approaches are very useful in establishing a particular model of new physics. However, even in the absence of new physics, a first detection of the CEνNS process (which is of substantial interest in its own right), and the accumulation of additional statistical resolution, will allow for the SM neutrino interactions to be studied in fine detail. Such observations are independent of the inverse β-decay detection mode, and provide access to those portions of the neutrino spectrum that are below the kinematic threshold for this process.

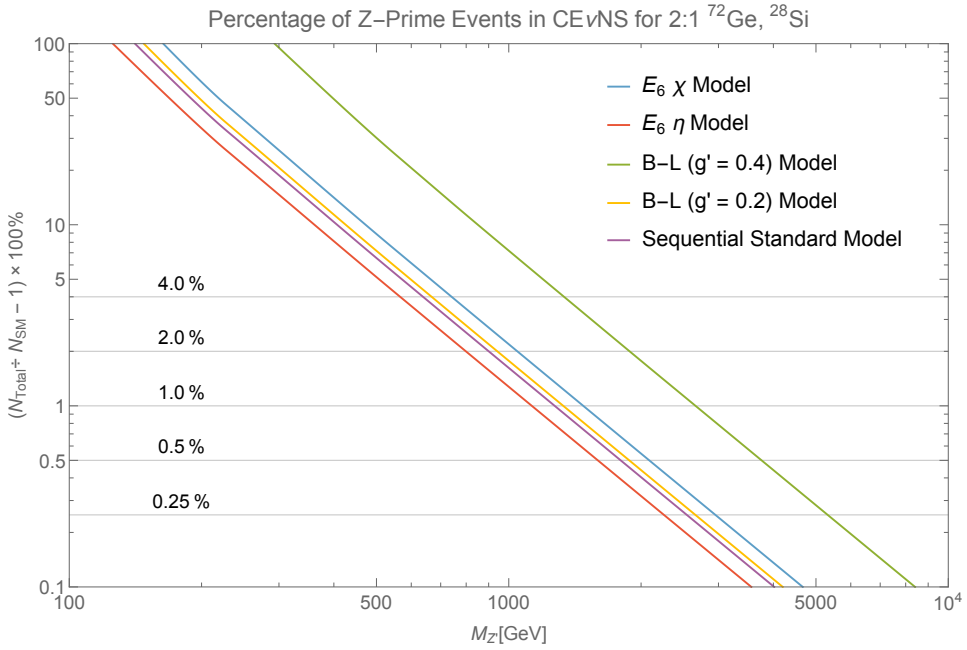

FIG. 5: Z' contributions to event rates in different models, as a fraction of the Standard Model Z-mediated background.

V. SENSITIVITY TO NEUTRINO NON-STANDARD INTERACTIONS AND MAGNETIC MOMENT

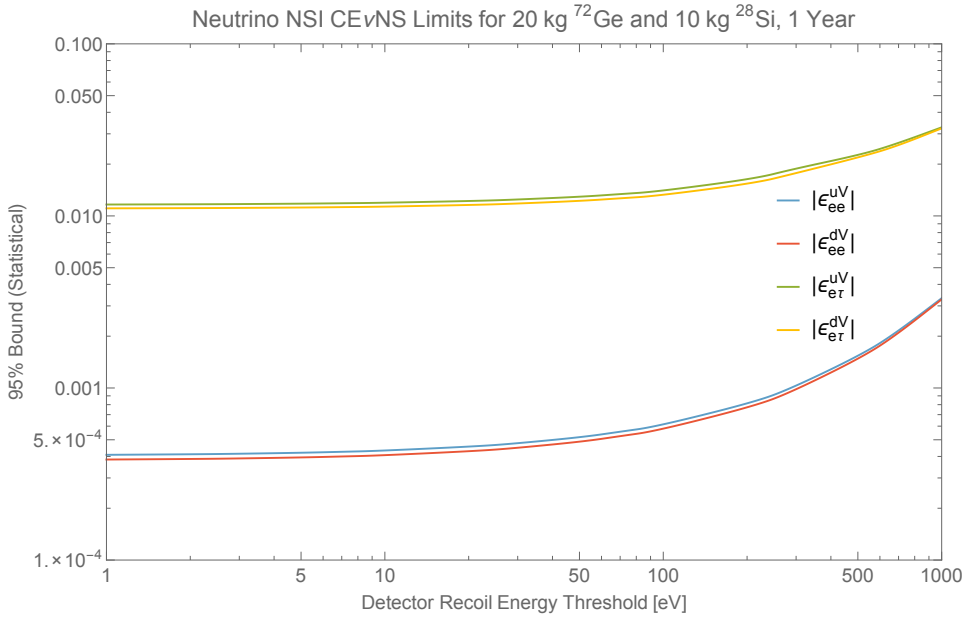

FIG. 6: Z' Sensitivity to non-standard neutrino interactions, including flavor-changing terms, in a low-mass ^{72}Ge and ^{28}Si detector.

In addition to the structured Z' contributions to the nuclear recoil rate, it is also possible to probe for generic non-standard neutrino interaction vertices [32, 50], both of the flavor-diagonal, and flavor-mixed varieties. We adopt the notation and normalization of Ref. [32], where, for example, ϵ_{ee}^{dV} is the coefficient for the diagonal e/e neutrino current with a down quark current (vector), and $\epsilon_{e\tau}^{uV}$ is the mixed e/τ neutrino current with an up quark. Note that the e/μ limits are very strong from flavor changing experiments [51], on the order of 10^{-7}, well beyond our ability to resolve. Existing e/e and e/τ limits are on the order of a few times 10^{-4} (cf. the second figure of Ref. [50]),

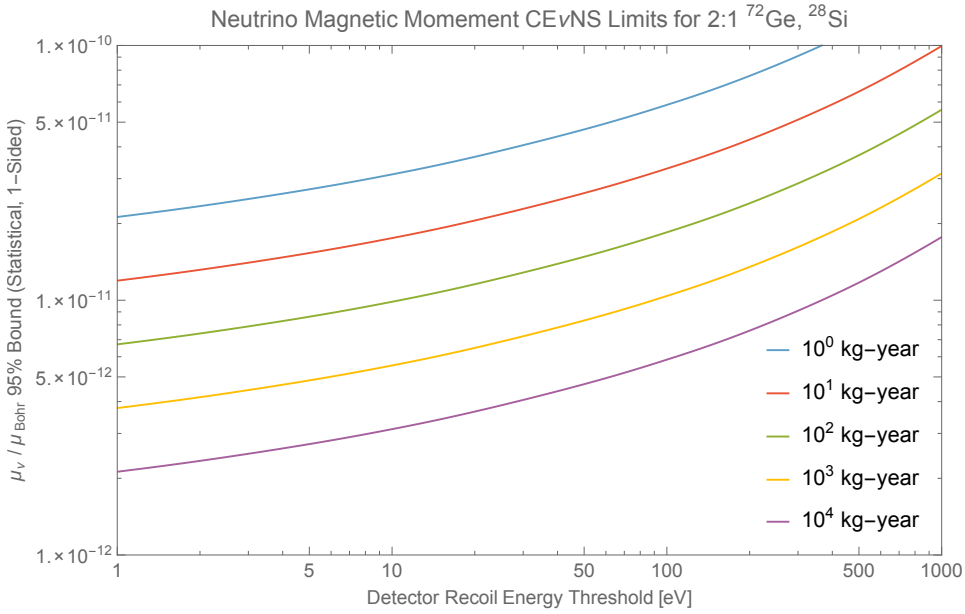

FIG. 7: Sensitivity to the neutrino magnetic moment ν_μ at various scalings of the detector mass and integration time.

converted to the Ref. [32] normalization. The e/e limits are of the order that may be competitively probed by a low-threshold nuclear recoil detector of the sort proposed, especially with modest extension of the target mass and/or integrated luminosity. Results are depicted in the Fig. (6) as a function of the detector recoil threshold $T_{\rm R}^{\rm th}$ for ^{72}Ge and ^{28}Si in a 2:1 mass ratio, with a combined mass of 30 kg, operating for a one-year continuous exposure, at 1 m from core. The modular design of the proposed detector array makes physical reconfiguration and up-scaling of the experiment relatively straightforward. For example, different ratios of ^{72}Ge and ^{28}Si may be employed to probe relative systematics, or to accentuate enhancements in the relative rate of a targeted BSM physics process. Prior caveats on systematic errors, and prior elaboration of the benefits of a differential search in both ^{72}Ge and ^{28}Si apply in this case as well.

It has historically been interesting to consider mutual limits on pairs of NSI parameters, allowing for interference [32, 52]. For example, if one considers down-type NSI coefficients with electron-electron and electron-tau flavor mixing [53] then the expected event rate is approximately proportional to $[N g_V^N + (Z+2N)\,\epsilon_{ee}^{dV}]^2 + [(Z+2N)\,\epsilon_{e\tau}^{dV}]^2$. There will be a circular ring of solutions in the $\{\epsilon_{ee}^{dV}\,,\,\epsilon_{e\tau}^{dV}\}$ plane centered at the coordinate $\{-N/(Z+2N)\,g_V^N, 0\}$, and intersecting the origin $\{0,0\}$, for which the SM event rate is replicated by conspiracy between the offsetting NSI parameters. The extension of this ring about its displaced center is manifestly symmetric with respect to the axes. Modulo some thickness appropriated to systematic and statistical errors, the ring divides discernible under-production (interior) from discernible over-production (exterior). However, realization of this scenario requires that the NSI coefficients are comparable in size to $g_V^N \equiv -1/2$, which is no longer experimentally tenable [50]. Restricting to parameterizations $\epsilon_{e[e,\tau]}^{dV} << g_V^N$ directly proximal to the origin, the previously described circle appears instead more like a vertical line or a gently inflecting parabola, indicating strongly preferential sensitivity to displacement along the horizontal (flavor-diagonal) coordinate. Moreover, there is intrinsic sensitivity to the sign of the flavor-diagonal term (with essentially identical sensitivity to magnitude) as distinguished by over/under production, which is not available for the off-diagonal (always over produces) coefficient. In this context, limits for leading flavor-diagonal terms decouple from the value of flavor-mixing NSI coefficients.

The described absence of competitive experimental bounds for the off-diagonal e/τ flavor changing interaction is somewhat paradoxical. In general, we emphasize that sensitivity of a nuclear recoil detector suffers when probing very weak interactions that are expressly prohibited by SM symmetries. This is regime where conventional experiments typically thrive because of low competing backgrounds, but there is no straightforward mechanism in this case for discriminating the flavor structure of the underlying interaction vertex on an event-by-event basis. Given sensitivity only to net deviations from an expected count of SM events, the underlying difficulty may be recast algebraically as an absence of rate-boosting SM cross-terms after squaring of the interaction amplitude. For example, the leading deviation for the scenario from the prior paragraph will come from a term proportional to $2N(Z+2N)\,g_V^N \epsilon_{ee}^{dV}$, which is only linear in the small term ϵ_{ee}^{dV}. Not only is the initial rate worse (like a square) for the off diagonal coefficients,

but the scaling of bounds with respect to luminosity integration is also less steep, like $\mathcal{L}^{1/4}$ rather than $\mathcal{L}^{1/2}$.

Coherent nuclear scattering is likewise a promising channel for probing the existence of a Majorana neutrino magnetic moment μ_ν [11]. Fig. (7) shows statistical search limits for the magnetic moment, using only the leading (at low threshold) nuclear CEνNS contributions. ^{72}Ge and ^{28}Si are combined in a 2:1 mass ratio. For one unified kg-year, at a detector recoil threshold $T_{\rm R}^{\rm th} = 10$ eV, the limit is about 3×10^{-11}, in units of the Bohr magneton. This is comparable to the present limits from terrestrial experiments [54]. The scaling with mass and time will again be a fourth-root. For 10^4 kg-years, the limit is down to about 3×10^{-12}, which is competitive with astrophysics sensitivity [55]. As before, however, systematic errors will play a limiting role. The event rate is proportional to just the nuclear proton count Z, whereas the base CEνNS strongly integrates the count of neutrons, so that differential comparison of ^{72}Ge and ^{28}Si is again very useful here to distinguish the origin of any observed event excess; likewise, this will provide for cancellation in correlated uncertainties.

VI. CANCELLATION OF SYSTEMATIC ERRORS IN DIFFERENTIAL EVENT RATES

In this section, we extend the former presentation of absolute scale sensitivities to new physics via CEνNS to highlight the benefits of differential CEνNS event rate observations (cf. the approach of Ref. [32]) in multiple nuclei to the cancellation of persistent systematic errors. In particular, the combination of silicon and germanium detector elements presents the opportunity to cleanly distinguish between various models and modes of new physics, based upon variations in the relative coupling strength to neutrons and protons. While intrinsically insensitive to, for example, the Z' mass or the size of the neutrino magnetic moment μ_ν, this approach can reveal very clear qualitative differences between the SM and various candidates for new physics, in a manner that cuts through the systematic uncertainty ceiling, recovering the potential science impact of large integrated luminosities.

We introduce the observables

$$\xi \equiv \frac{E_{\rm Ge} \,/\, B_{\rm Ge} \,-\, 1}{E_{\rm Si} \,/\, B_{\rm Si} \,-\, 1} = \frac{S_{\rm Ge} \,/\, B_{\rm Ge}}{S_{\rm Si} \,/\, B_{\rm Si}} \,, \tag{3}$$

and

$$\zeta \equiv \frac{E_{\rm Ge}}{B_{\rm Ge}} - \frac{E_{\rm Si}}{B_{\rm Si}} = \frac{S_{\rm Ge}}{B_{\rm Ge}} - \frac{S_{\rm Si}}{B_{\rm Si}} \,, \tag{4}$$

where E, B, and $S \equiv E - B$ are the experimental total, expected standard model background, and beyond standard model signal event counts, respectively. Table III itemizes signature values of the ξ statistic for various Z' model families, and also for nuclear scattering via the anti-neutrino magnetic moment μ_ν coupling. These distinctive signatures are broadly independent of the underlying mass scale ($M_{Z'}$), mixing angle (β), or coupling strength (g'). The ζ statistic retains sensitivity to the new physics scale, while still allowing for the cancellation of systematic errors.

TABLE III: The Eq. (3) ratio ξ of normalized BSM event counts in ^{72}Ge and ^{28}Si at a detector recoil threshold $T_{\rm R}^{\rm th} = 10$ eV.

	SM	E_6	$B-L$	μ_ν
ξ	1.0	0.89	0.86	0.43

We adopt the point of view that the theoretically calculated background counts B are absolute, with zero error ($\delta B = 0$). This is not to say, of course, that the calculation inherits no propagated uncertainty, but rather that differences between theory and experiment are considered to be absorbed by the experimental side. Consequently, $\delta S = \delta E$. Variations of the statistics in Eqs. (3,4) are then given as follows.

$$\frac{\delta\xi}{\xi} = \frac{\delta E_{\rm Ge}}{E_{\rm Ge} - B_{\rm Ge}} - \frac{\delta E_{\rm Si}}{E_{\rm Si} - B_{\rm Si}} \quad ; \quad \delta\zeta = \frac{\delta E_{\rm Ge}}{B_{\rm Ge}} - \frac{\delta E_{\rm Si}}{B_{\rm Si}} \tag{5}$$

Variations $\delta E = \delta E_{\rm Syst} + \delta E_{\rm Stat}$ will generically be composed of both systematic and statistical components. The systematic term is expected to be primarily correlated across detectors, such that $\delta E_{\rm Ge}/E_{\rm Ge} \simeq \delta E_{\rm Si}/E_{\rm Si}$. Noting that the new physics contribution is generically expected to be small, i.e. $E \simeq B$, it is observed that systematic effects cancel to leading order in both terms of Eq. (5), as expected. Moreover, the residual statistical uncertainties

$\delta E_{\rm Stat} \simeq \sqrt{B}$ may be estimated as a root of the ambient SM background. Combining these uncorrelated statistical terms in quadrature, estimates of the standard uncertainty σ for ξ, ζ emerge.

$$\frac{\sigma_\xi}{\xi} = \sqrt{\frac{B_{\rm Ge}}{S^2_{\rm Ge}} + \frac{B_{\rm Si}}{S^2_{\rm Si}}} \quad ; \quad \sigma_\zeta = \sqrt{\frac{1}{B_{\rm Ge}} + \frac{1}{B_{\rm Si}}} \tag{6}$$

The percentage error in both ξ and ζ is observed to scale like $\mathcal{L}^{-1/2}$ with luminosity.

VII. CONCLUSIONS

We have discussed the prospects for probing BSM physics, in particular Z' and non-standard neutrino interactions, as well as the magnetic moment of the neutrino, using ultra-low threshold (~ 10 eV) ^{72}Ge and ^{28}Si detectors [12]. This analysis is motivated by a developing experimental program in cooperation with the Nuclear Science Center at Texas A&M University. We have highlighted the benefit of combining silicon and germanium detectors, which helps to distinguish between candidates for new physics by leveraging distinctive couplings to neutrons vs. protons; the benefits of this approach to bypassing the systematic error wall have also been emphasized. The projected sensitivities to Z' and non-standard neutrino interactions are complementary to ongoing searches for new physics at the LHC, especially with regards to the capacity for discrimination between different models of Z' physics in the large statistics limit; by extension, this specifically includes potential explanations of the diboson excess currently reported by both CMS and ATLAS that are based upon a leptophobic $B-L$ type Z'. We find that the projected constraints on the neutrino magnetic moment will improve upon the terrestrial bound, and can become competitive with astrophysical bounds. A summary of (statistical) bounds on leading modes of BSM physics considered in this paper is presented in Table IV. Limits for the $B-L$ model with $g' = 0.2$, as well as for the E_6 η-model and the SSM, are order-comparable with the exhibited E_6 χ-model. Scenarios for substantially scaling up the initial mass-time exposure are tabulated. Systematic errors are comparable to statistical errors for the baseline scenario, but substantially dominate in the latter cases; this effect may be mitigated by careful application of differential event rates. The limits for Z' are not greatly dependent upon the specific detector threshold, as long as it is not too far above 100 eV. By contrast, the magnetic moment limits thrive with a very low-threshold detector, of the type described.

In addition to the probes of BSM physics discussed here, ultra-low threshold detectors can be utilized in searches for sterile neutrinos, and the detection of low energy neutrinos from the Sun. Dedicated analyses will be presented in forthcoming publications.

TABLE IV: Summary of approximate statistical sensitivity to new physics in a 2:1 ^{72}Ge, ^{28}Si detector with recoil threshold $T_{\rm R}^{\rm th} = 10$ eV. Various integrated mass-time exposures are considered, starting with near-term plans for an order 30 kg detector operating for 1 year, and scaling up to 1,000 kg for 5 years, and 10,000 kg for 10 years. Z-prime masses are in TeV.

kg-years	$M_{Z'}(E_6, \chi)$	$M_{Z'}(B-L, g'=0.4)$	$\mu_\nu/\mu_{\rm Bohr}$
30	2.4	4.3	1.3×10^{-11}
5×10^3	8.5	15	3.7×10^{-12}
1×10^5	18	32	1.8×10^{-12}

Acknowledgments - The authors acknowledge very useful discussions with Nader Mirabolfathi, Rusty Harris, and Grigory Rogachev. BD acknowledges support from DOE Grant DE-FG02-13ER42020. LES acknowledges support from NSF grant PHY-1522717. JWW acknowledges support from the Mitchell Institute for Fundamental Physics and Astronomy, NSF grant PHY-1521105, and the SHSU Department of Physics.

[1] D. Z. Freedman, Phys. Rev. **D9**, 1389 (1974).
[2] D. Z. Freedman, D. N. Schramm, and D. L. Tubbs, Ann. Rev. Nucl. Part. Sci. **27**, 167 (1977).
[3] B. Cabrera, L. M. Krauss, and F. Wilczek, Phys. Rev. Lett. **55**, 25 (1985).
[4] J. Monroe and P. Fisher, Phys. Rev. **D76**, 033007 (2007), 0706.3019.
[5] L. E. Strigari, New J. Phys. **11**, 105011 (2009), 0903.3630.

[6] J. Billard, L. Strigari, and E. Figueroa-Feliciano, Phys. Rev. **D89**, 023524 (2014), 1307.5458.
[7] M. Pospelov, Phys. Rev. **D84**, 085008 (2011), 1103.3261.
[8] R. Harnik, J. Kopp, and P. A. N. Machado, JCAP **1207**, 026 (2012), 1202.6073.
[9] J. Barranco, O. G. Miranda, and T. I. Rashba, Phys. Rev. **D76**, 073008 (2007), hep-ph/0702175.
[10] C. Adams et al., in *Workshop on the Intermediate Neutrino Program (WINP 2015) Upton, NY, USA, February 4-6, 2015* (2015), 1503.06637, URL `http://inspirehep.net/record/1355214/files/arXiv:1503.06637.pdf`.
[11] T. S. Kosmas, O. G. Miranda, D. K. Papoulias, M. Tortola, and J. W. F. Valle, Phys. Rev. **D92**, 013011 (2015), 1505.03202.
[12] N. Mirabolfathi, H. R. Harris, R. Mahapatra, K. Sundqvist, A. Jastram, B. Serfass, D. Faiez, and B. Sadoulet (2015), 1510.00999.
[13] H. T. Wong, J. Li, and Z. Y. Zhou (TEXONO), in *1st Yamada Symposium on Neutrinos and Dark Matter in Physics (YS-1 and NDM03) Nara, Japan, June 9-14, 2003* (2003), hep-ex/0307001.
[14] e. a. Goorley, T., Nucl. Tech. **180**, 298 (2012).
[15] V. Kopeikin, L. Mikaelyan, and V. Sinev, Phys. Atom. Nucl. **67**, 1892 (2004), [Yad. Fiz.67,1916(2004)], hep-ph/0410100.
[16] P. Vogel, G. K. Schenter, F. M. Mann, and R. E. Schenter, Phys. Rev. **C24**, 1543 (1981).
[17] V. I. Kopeikin, Phys. Atom. Nucl. **75**, 143 (2012), [Yad. Fiz.75N2,165(2012)].
[18] K. Schreckenbach, G. Colvin, W. Gelletly, and F. Von Feilitzsch, Phys. Lett. **B160**, 325 (1985).
[19] P. Venkataramaiah, K. Gopala, A. Basavaraju, S. S. Suryanarayana, and H. Sanjeeviah, Journal of Physics G: Nuclear Physics **11**, 359 (1985).
[20] F. Von Feilitzsch, A. A. Hahn, and K. Schreckenbach, Phys. Lett. **B118**, 162 (1982).
[21] A. A. Hahn, K. Schreckenbach, G. Colvin, B. Krusche, W. Gelletly, and F. Von Feilitzsch, Phys. Lett. **B218**, 365 (1989).
[22] T. A. Mueller et al., Phys. Rev. **C83**, 054615 (2011), 1101.2663.
[23] H.-B. Li and H. T. Wong, J. Phys. **G28**, 1453 (2002), hep-ex/0111002.
[24] G. McLaughlin, AIP Conf. Proc. **1666**, 160001 (2015).
[25] D. Akimov et al. (COHERENT) (2015), 1509.08702.
[26] J. Alonso et al. (2010), 1006.0260.
[27] V. Singh and H. T. Wong (TEXONO), PoS **AHEP2003**, 053 (2003), nucl-ex/0412057.
[28] H. T. Wong, H.-B. Li, J. Li, Q. Yue, and Z.-Y. Zhou, J. Phys. Conf. Ser. **39**, 266 (2006), [,344(2005)], hep-ex/0511001.
[29] A. K. Soma et al. (TEXONO) (2014), 1411.4802.
[30] P. S. Barbeau, J. I. Collar, and O. Tench, JCAP **0709**, 009 (2007), nucl-ex/0701012.
[31] P. Vogel and J. Engel, Phys. Rev. **D39**, 3378 (1989).
[32] J. Barranco, O. G. Miranda, and T. I. Rashba, JHEP **12**, 021 (2005), hep-ph/0508299.
[33] L. M. Sehgal and M. Wanninger, Phys. Lett. **B171**, 107 (1986).
[34] S. J. Brice et al., Phys. Rev. **D89**, 072004 (2014), 1311.5958.
[35] J. Engel, Phys. Lett. **B264**, 114 (1991).
[36] S. Eidelman et al. (Particle Data Group), Phys. Lett. **B592**, 1 (2004).
[37] R. W. Robinett and J. L. Rosner, Phys. Rev. **D26**, 2396 (1982).
[38] J. L. Hewett and T. G. Rizzo, Phys. Rept. **183**, 193 (1989).
[39] M. Carena, A. Daleo, B. A. Dobrescu, and T. M. P. Tait, Phys. Rev. **D70**, 093009 (2004), hep-ph/0408098.
[40] P. Langacker, Rev. Mod. Phys. **81**, 1199 (2009), 0801.1345.
[41] R. Laha, B. Dasgupta, and J. F. Beacom, Phys. Rev. **D89**, 093025 (2014), 1304.3460.
[42] K. C. Y. Ng and J. F. Beacom, Phys. Rev. **D90**, 065035 (2014), [Erratum: Phys. Rev.D90,no.8,089904(2014)], 1404.2288.
[43] L. Basso, A. Belyaev, S. Moretti, G. M. Pruna, and C. H. Shepherd-Themistocleous, PoS **EPS-HEP2009**, 242 (2009), 0909.3113.
[44] L. Basso, A. Belyaev, S. Moretti, G. M. Pruna, and C. H. Shepherd-Themistocleous, Eur. Phys. J. **C71**, 1613 (2011), 1002.3586.
[45] Y. Gershtein et al., in *Community Summer Study 2013: Snowmass on the Mississippi (CSS2013) Minneapolis, MN, USA, July 29-August 6, 2013* (2013), 1311.0299, URL `http://inspirehep.net/record/1263192/files/arXiv:1311.0299.pdf`.
[46] J. Cao, Nucl. Phys. Proc. Suppl. **229-232**, 205 (2012), 1101.2266.
[47] G. Aad et al. (ATLAS) (2015), 1506.00962.
[48] V. Khachatryan et al. (CMS), JHEP **08**, 173 (2014), 1405.1994.
[49] Y. Gao, T. Ghosh, K. Sinha, and J.-H. Yu (2015), 1506.07511.
[50] M. B. Wise and Y. Zhang, Phys. Rev. **D90**, 053005 (2014), 1404.4663.
[51] S. Davidson, C. Pena-Garay, N. Rius, and A. Santamaria, JHEP **03**, 011 (2003), hep-ph/0302093.
[52] K. Scholberg, Phys. Rev. **D73**, 033005 (2006), hep-ex/0511042.
[53] P. S. Amanik, G. M. Fuller, and B. Grinstein, Astropart. Phys. **24**, 160 (2005), hep-ph/0407130.
[54] A. G. Beda, V. B. Brudanin, V. G. Egorov, D. V. Medvedev, V. S. Pogosov, M. V. Shirchenko, and A. S. Starostin (2010), 1005.2736.
[55] G. G. Raffelt, *Stars as laboratories for fundamental physics* (1996), ISBN 9780226702728, URL `http://wwwth.mpp.mpg.de/members/raffelt/mypapers/199613.pdf`.